

RESEARCH

Open Access



5G IoT-based geohazard monitoring and early warning system and its application

Zhaohua Li^{1,2}, Linqun Fang^{2*}, Xiaokun Sun³ and Wang Peng⁴

*Correspondence:

254148376@qq.com

²Yunnan Innovation Institute,
BUAA, Kunming 650233,
China

Full list of author information
is available at the end of the
article

Abstract

With the expansion of human production activities, geological disasters caused by slope instability are occurring more frequently. Hence, the research on effective monitoring and forecasting of the geotechnical stability of slopes is of great significance for the prevention and mitigation of slope geological disasters. In this study, a landslide monitoring and early warning system based on 5G Internet of Things (IoT) technology is introduced. The system monitors important indicators such as three-dimensional surface displacement, rainfall, and ground cracks using Global Navigation Satellite System equipment and various IoT sensors deployed on site. The key monitoring data are transmitted and displayed by 5G communication and advanced data visualization technologies. An early warning guideline is established by combining the surface deformation rate–time curve according to a four-level early warning method as well as embedded vector maps such as the topographic and geomorphological remote sensing map of the monitoring area, the geological section map, and the monitoring point distribution map. The system has the functions of accurate acquisition, rapid transmission, automatic search, and comprehensive analysis and is applied to the study of creep slopes of the Lianhe terraces in Youxi County, Fujian Province, with remarkable results.

Keywords: Geological disasters, 5G communication, IoT, Monitoring and early warning, GNSS

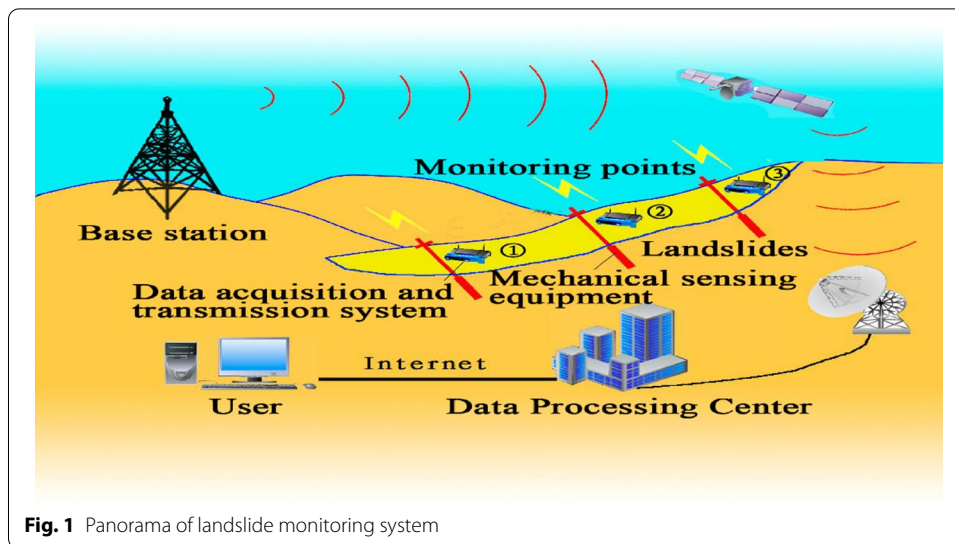
1 Introduction

Landslides and other geological disasters are increasingly becoming a key issue worldwide [1–5], and China is one of the countries in the world that are more seriously affected by geological disasters. Geological disasters involve complex geological conditions, the geographical environment, large spatiotemporal differences in climate, and many hidden and widely distributed geological hazards, which are destructive and occur suddenly. As a result of both natural events and human activities, especially the rapid development of society, the economy, and cities in recent years, destructive geological disasters are occurring more frequently. This causes significant impact and damage to the social and economic development and the safety of people's lives and properties, directly threatening the ecological environment on which human beings depend. According to relevant statistics, at least 400 cities, counties, districts, towns, and more

than 10,000 villages in China are threatened by various types of geological disasters, encompassing a total area of 1,735,200 square kilometers and accounting for 18.10% of the total land area of China. Examples include the six satiated loess landslides induced by continuous rainfall on August 21, 1981 [6], loess mudflow landslides caused by agricultural irrigation in Hefangtai [7], high-speed loess landslides induced by irrigation in Huaxian County, Shaanxi in 2006 [8], Donghekou landslides induced by the Wenchuan earthquake in 2008 [10], high-speed remote landslides that killed 46 people in Zhenxiong, Yunnan in 2013 [9, 11, 12], and the runoff landslide in 2015 at the sludge receiving site in Guangming New District, Shenzhen [13–15]. With the rapid economic development in recent years and the high population density in China, each occurrence of a geological disaster may result in great loss of life and property to the disaster-affected area. Therefore, it is of high practical application and educational value to carry out monitoring, early warning, and risk assessment of geological disasters on a continuous basis and to establish an integrated all-year-round monitoring, early warning, and risk assessment system.

Owing to equipment limitations in the early days, monitoring of geological disasters such as landslides was mainly based on the manual observation of surface change characteristics and anomalies in groundwater and the surrounding flora and fauna to determine the likelihood of an occurrence by inference [16, 17]. Later, with the development of technological, conventional instruments of surface displacement monitoring, including total station, theodolite, level gauge, GPS monitoring, the newly developed GPS mobile phone monitoring, and Interferometric Synthetic Aperture Radar (InSAR) technology, new instruments have gradually been utilized [18–22]. Currently, Global Navigation Satellite System (GNSS) monitoring methods based on point data acquisition and the space-borne and discontinuous ground-based InSAR techniques based on surface data acquisition are widely used to monitor large-scale landslides and have also resulted in great progress in landslide monitoring and prediction [23–25]. 5G communication and IoT technologies are the key points to establish an efficient remote-monitoring system of geological disasters. Compared with the older techniques, the 5G communication provides a higher speed, larger capacity and lower latency, and the IoT allows to interconnect diversified sensors in one framework to synthetically analyze and assess a problem. In consideration of the abovementioned techniques, the remote-monitoring system is applied more and more frequently. A typical monitoring system of landslide is shown as in Fig. 1. Relevant sensors are installed in the field to obtain the necessary data, which are remotely transmitted and stored in servers. After the analysis according to the landslide criterion, the corresponding warning can be sent. Recently, along with the rapid development of 5G communication technology, a novel monitoring and prediction system based on 5G-IoT was developed and applied in a slope with long-term creep located in a terrace field.

This paper describes in detail this landslide monitoring and early warning system based on 5G-IoT technology. The system monitors important indicators such as three-dimensional surface displacement, rainfall, and ground cracks through GNSS equipment and various IoT sensors deployed on site, transmitting key monitoring data with 5G communication technology, which are displayed with advanced data visualization technology. An early warning guideline is established in accordance with a four-level



early warning method by combining the surface deformation rate–time curve as well as embedded vector maps such as topographic and geomorphological remote sensing maps of the monitoring area, the geological section map, and the monitoring point distribution map. The system has the functions of accurate acquisition, rapid transmission, automatic search, and comprehensive analysis. This paper is divided into four sections. The second section gives a detailed introduction of the geo-meteorological and hydro-geological conditions at the pilot site as well as the current situation of the slow creeping terrace slope. The third section introduces the new monitoring and early warning system of geological disasters and its application in this slope. The fourth section presents a brief summary of the study.

2 Methods/experimental

2.1 Background of the Youxi terraces landslide area

Youxi County is located south of the 26th parallel north and about 100 km east of the East China Sea, with a humid mid-subtropical monsoon climate. Its summer is warm/hot, winter is cool/chilly, and spring and summer are rainy, with abundant precipitation. The average annual precipitation is between 1500 and 1750 mm, with extremely uneven rainfall throughout the year, including many typhoons and rainstorms from May to August, which is the main flood season.

Lianhe Township of Youxi County is surrounded by mountains, with an elevation of 260–1137.6 m, and a medium–low hilly landform. The relative elevation difference is 877.6 m, and the slope has a gradient of 25°–45°. The mountainous terrain is high with steep topography and sharp gully cutting. According to the regional 1/50,000-scale geological survey report (G50E010017), the fold structures developed in the area of Lianhe Township, Youxi County, are mainly located in the Nanping-Yuxi compound syncline, with the axis located in the area of Xiqin, pointing in the 20°–30° northeast direction. The area is composed mainly of Presinian strata, with a gentle dip of about 30° in the axis of the rock layer, while the flank can reach 50°–60°. The secondary fold structures are developed in the axial part of the compound syncline and are parallelly arranged in

the northeast direction. The fault structures in the area include mainly two groups: the north–northeast fault structure of Baizhangji in Wencheng County and the northwest fault structure of Dingdi in the highlands, with the former being the main fault structure. These two groups of fault structures are large in scale, generally extending up to tens of kilometers, cutting deep into different tectonic layers. In the fault structures, extrusion, rushing zones, and conglomerate are normally distributed, while silicification, chloritization, and other alterations are generally observed with the development of small fractures. The Youxi Lianhe terraces are located at the intersection of these two fault structures, with fragmented and unstable rock layers (Fig. 2).

The Youxi Lianhe terraces have a history of 1300 years and are one of the earliest large-scale ancient terraces dug by the Han people in the history of China. The relative elevation difference of the terraced landslide area is 877.6 m, and the slope gradient is 25°–45°. The area has a medium–low hilly landscape, with abundant rainfall all year round or seasonally, and the geological environment is relatively fragile. According to the statistics of “Fujian Province Geological Disaster Prevention and Control Information Network,” in the Lianhe Town of Youxi County, there are 105 locations of potential geological disaster and 68 locations of high and steep slopes. The core area of the Youxi Lianhe terraces connects the five administrative villages of Lianxi, Dongbian, Lianyun, Yunshan, and Xiaoyun, with 27 locations of potential landslide, among which, Yunshan and Lianyun are along the 016 rural road, which has three existing locations of pulling deformation with serious faults on the pavement, which may result in potentially large-scale landslides. Every year during the flood season there are geological disasters of different degrees, including the most typical landslide or mudslide disaster that occurred in

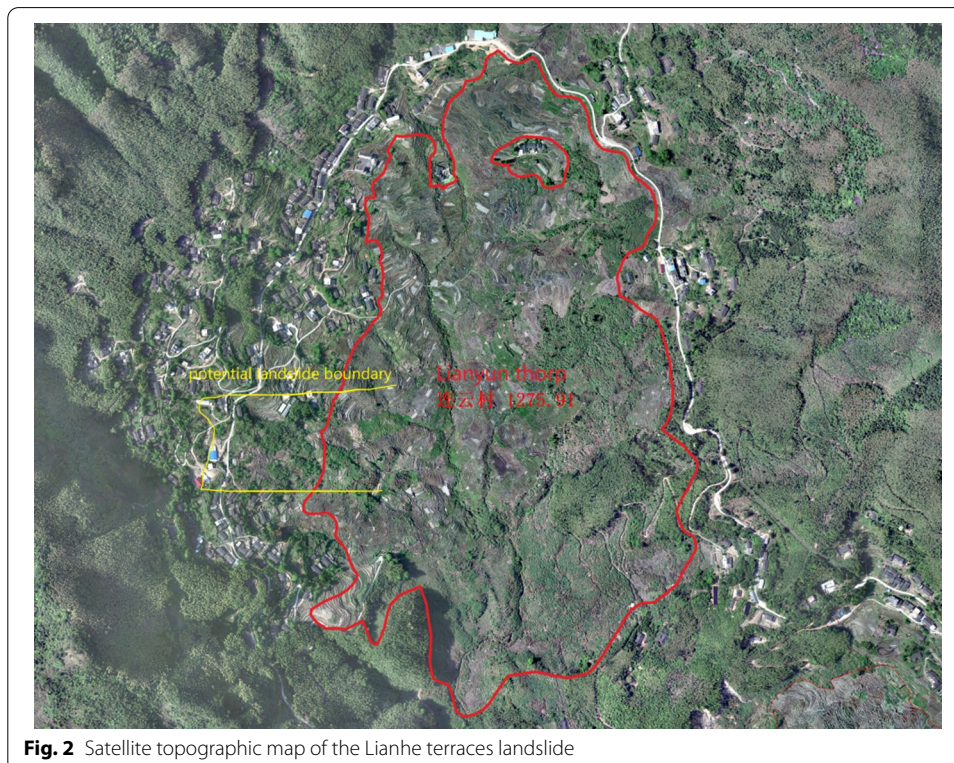


Fig. 2 Satellite topographic map of the Lianhe terraces landslide

2010 in Xiaoyun, destroying approximately 110,000 square meters of terraced rice fields to varying degrees. The influence of the geological environment on the terraced rice field ecosystem is progressively noticeable, as the situation becomes increasingly serious (Fig. 3).

According to the field survey, the overall slope of the terraces in Lianyun is 6.53° – 35.87° , the minimum annual deformation rate along the slope is 13.04 mm, the maximum annual deformation rate is 165.28 mm, and the average throughout the years is 57.55 mm. The overall slope of the terraces in Yunshan is 5.22° – 38.04° , the minimum annual deformation rate along the slope is 10.02 mm, the maximum annual deformation rate is 148.79 mm, and the average throughout the years is 30.42 mm. The overall slope of the terraces in Dongbian is 5.39° – 28.26° , the minimum annual deformation rate is 10.0 mm, the maximum annual deformation rate is 148.75 mm, and the average throughout the years is 32.97 mm.

The creeping of the terraced slope on the east side of Lianyun has been most severe in recent years. According to the preliminary site survey, although the ground cracks on the back edge of the landslide developed only slightly, cracks are evident in the buildings and roads of greater stiffness. While the main structure of the Lin's ancestral hall at the back edge of the landslide is intact and no cracks are observed, the crack between the main structure and the auxiliary structure is obvious (Fig. 4). The tensioned ground cracks near the blue-topped shed in the northeast direction continue to extend on the surface, and the direction of the fissure is basically parallel to the slope direction (Fig. 4). Obvious cracks can be observed on the road surface nearby, which are mainly induced by the sunken slabs at the back edge (Fig. 5). In addition, shear cracks of an echelon arrangement are observed on the concrete floor of a pig farm in the east part of the

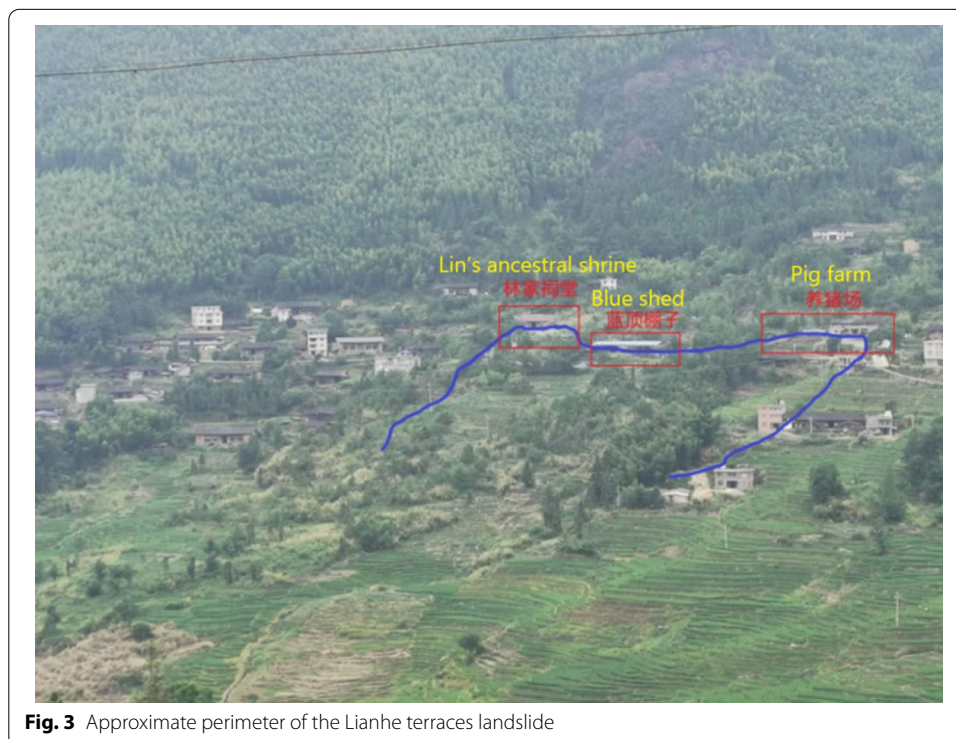


Fig. 3 Approximate perimeter of the Lianhe terraces landslide



village. The landslide has caused a slight subsidence of the slabs at the back edge, and the front edge is located in the terraced area, with bulging at some locations. The main surface cracks are distributed in a scattered manner. The perimeter of the landslide is not clear; currently, the landslide is in a slow creeping state without having entered the accelerated deformation stage.

2.2 IoT-based monitoring and early warning system and its application

Based on the above-mentioned potential hazards caused by landslide in the later stages and the need for effective monitoring and early warning, the latest 5G and IoT technologies are combined to establish a landslide remote monitoring and early



Fig. 5 Road cracking at the landslide body in Lianyun Village

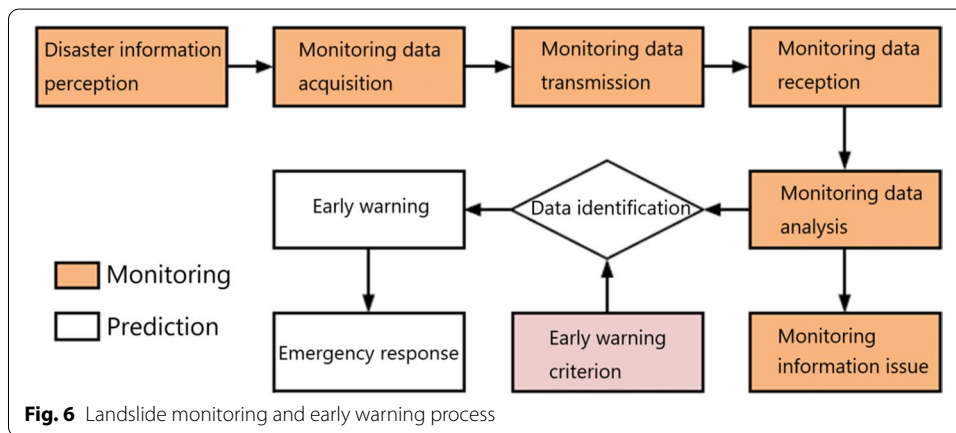


Fig. 6 Landslide monitoring and early warning process

warning system for long-term monitoring and early warning. The deformation and destruction trend of the landslide body are tracked in real time, so as to discover and forecast dangerous situations in time for mitigating measures to prevent the loss of life and property caused by sudden disasters.

A complete landslide monitoring system includes data sensing, acquisition, transmission, reception, processing, analysis, and information release mechanism, while a complete landslide early warning system includes data sensing, acquisition, transmission, reception, processing, analysis (judgment), early warning, and response. Therefore, the main differences between monitoring and early warning are the evaluation of the monitoring data according to the early warning guideline and the timely issuance of early warning and risk avoidance responses, as shown in Fig. 6. It is necessary for the landslide monitoring and early warning systems to be able to have automatic identification and judgment functions, according to the early warning guideline, and automatic issuance of early warning information. In this paper, the 5G, IoT and landslide early warning technologies are integrated in one monitoring system. The monitoring data are obtained and read by monitoring stations (rainfall, ground fissure, ground deformation...) in the field. They are transmitted then by 5G and analyzed in servers. Finally, the early warning can be sent according to the effective warning criterion for gradual landslides.

2.2.1 Data acquisition

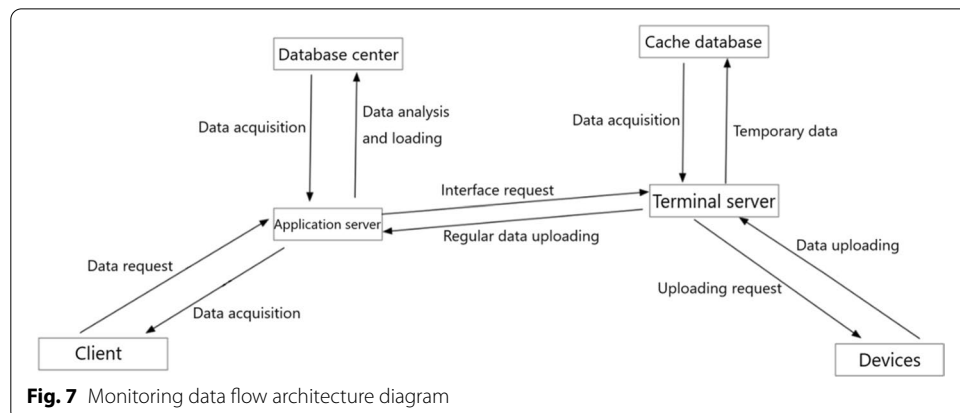
The data of the system come from the regular data acquisition with the equipment. At present, the system supports automatic monitoring equipment for GNSS-based 3D surface displacement, rainfall, cracks, groundwater level, second-order power, etc. The equipment communicates directly with the equipment-side server, and the collected data are regularly transmitted to the equipment-side server through the network.

To facilitate data exchange with the application-side server, the equipment-side server uses a cache database and periodically transmits data to the application-side server according to the data request specification of the application-side server. After the application-side server receives the data transmitted from the equipment-side server, the data are pre-processed before entering into the storage center database (see Fig. 7 for the data flow architecture).

The user side can request to query the data of the application-side server through the HTTP protocol. Both query by time range and query by specified equipment type are supported. The application-side server will automatically aggregate the data according to the time range of the query. For equipment-specific data that calculate relative values (such as data of GNSS equipment and crack detection equipment), the system automatically calculates the relative data values based on the reference time of the location of the monitoring equipment.

2.2.2 Data transmission

As the latest breakthrough in communication field, 5G communication has present many advantages such as high speed, large capacity, and low latency. In the IoT, high-quality and real-time monitored data transmission is often necessary. In particular, many IoT terminal devices will play an important role in the 5G communication system, such as autonomous driving or a surveillance system with a high-definition camera. In 5G networks, a multilayer structure will be considered, owing to the heterogeneity of equipment and services. Regarding the IoT, it is a potential technology to realize the interconnection of all things. The popularity of small and inexpensive computing devices with sensing and communication functions is paving the way for the widespread application of IoT [28]. In the monitoring and prediction project of Youxi landslide, the



corresponding IoT terminals are used to monitor rainfall, ground fissure and surface deformations in real time, and then 5G communication channels are chosen to transmit data.

An automatic data acquisition equipment was developed based on the data output interface and communication protocol of a high-precision mechanics sensor. The equipment includes a data acquisition module, a data storage module, a data transmission module, and a solar power supply equipment. The data acquisition equipment is connected to the sensors and the solar power supply system through shielded cables to form a complete data acquisition system.

In order to improve the stability and reliability of data transmission, each monitoring location in the monitoring area is connected with wireless sensor network technology, and the data are transmitted centrally from the field to the indoor monitoring center using the dual communication mode of BeiDou satellite and GPRS (referred to as BD/GPRS mode) after data acquisition.

There are two modes of aggregating data from monitoring locations within the monitoring area, with the mesh networking mode and the linear networking mode.

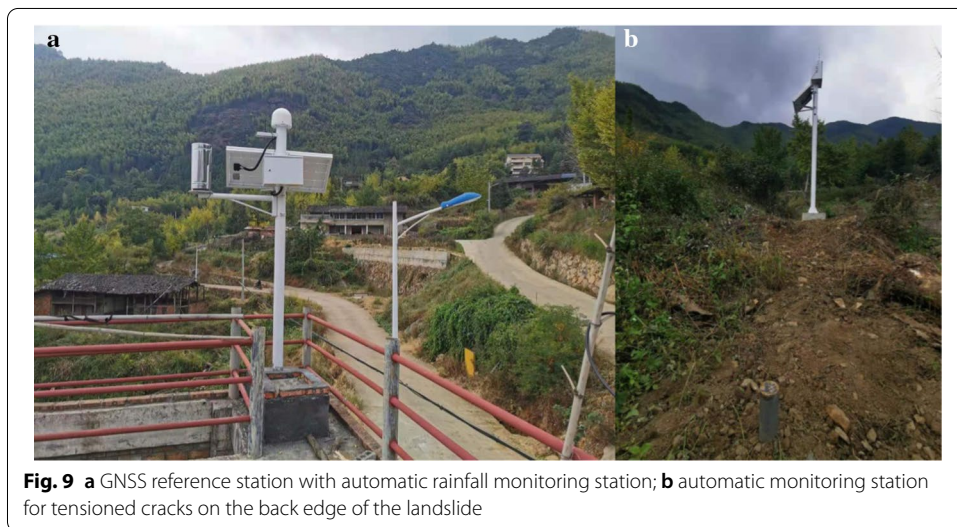
1. Mesh networking mode: monitoring locations (nodes) can be networked for data transmission at will within the effective range. When one of the monitoring locations fails, other adjacent monitoring locations can be selected for data transmission until the data are finally transmitted to the sink node. The advantage of this transmission mode is that the data transmission is secure, and the data transmission within the whole monitoring area will not be paralyzed due to the failure at one monitoring location (see Fig. 7).
2. Linear networking mode: monitoring location N_i and its effective proximity location N_{i-1} form a network, N_{i-1} and N_{i-2} form a network, and so on until communication between the monitoring location N_1 and the convergence point is obtained, such that data of the N locations on the same line are all converged to the convergence point. The advantage of this transmission mode is the long effective transmission distance, suitable for strip-shaped monitoring area. The disadvantage is that the data transmission stability is not guaranteed, when one of the nodes is damaged, the data transmission of the whole system is paralyzed.

Therefore, this system uses two transmission modes in a complementary form, which improves both the effective distance of data transmission and the security and stability of data transmission.

3 Results and discussion

3.1 Monitoring network at the Lianhe terraces landslide site in Youxi county

According to the local hydrogeological conditions and on-site survey, this case study is mainly based on monitoring of GNSS-based surface deformation, surface cracks, wall cracks, and rainfall. Additionally, monitoring data of pore water pressure and second-order power (equipment recommended to be installed at the accelerated deformation stage of the landslide) can be considered at a later stage based on the analysis of monitoring data. To facilitate comprehensive monitoring of the overall displacement due to



the landslide, a GNSS monitoring station was installed along each of the front, middle, and back edges of the landslide in a straight line (see Fig. 8), and a reference station was set at a stabilized rock body within 2 km of the landslide body. Since most landslides in this area are induced by rainfall during the rainy season, a rainfall monitoring station was set at the location of the GNSS reference station, as shown in Fig. 9a.

Taking GPS positioning used in this study, for example, relative positioning is most commonly used in static positioning of GPS measurement. In relative positioning, the vector of baseline will be calculated; that is, the position of one point in GPS control network relative to another can be obtained. This method is often used in GPS measurement with short baseline. In GPS relative positioning, the second difference of carrier phase observation is generally used as virtual observation. The adjustment calculation is carried out according to the principle of least square adjustment; therefore, this observation model can eliminate clock error. In addition, it can be known that the orbit error after double difference, ionosphere and the influence on the delay of current layer are very small and can even be ignored; thus, the observation model can be simplified. The positioning accuracy of this method is relatively high, which can be applied to engineering measurement.

In GPS relative positioning, the second difference observation of carrier phase observation is often used as the virtual observation value in baseline measurement. According to the least square principle, for epoch t , the observation equation of second difference from station i and j for satellite p and q is

$$\Delta \nabla \Phi_{ij}^{pq} = \nabla \Phi_{ij}^q - \nabla \Phi_{ij}^p = \Phi_j^q - \Phi_i^q - \Phi_j^p + \Phi_i^p \tag{1}$$

Suppose that at epoch t , stations i and j synchronously observe four satellites whose numbers are 1, 2, 3 and 4 in the sky, and set satellite 1 as the reference star. The matrix of the observation equation of quadratic difference can be expressed as:

$$\Delta \nabla \Phi = B \Phi \tag{2}$$

where

$$\Delta \nabla \Phi = \begin{bmatrix} \Delta \nabla \Phi_{ij}^{12} \\ \Delta \nabla \Phi_{ij}^{13} \\ \Delta \nabla \Phi_{ij}^{14} \end{bmatrix}, \quad B = \begin{bmatrix} 1 & -1 & -1 & 1 & 0 & 0 & 0 & 0 \\ 1 & -1 & 0 & 0 & -1 & 1 & 0 & 0 \\ 1 & -1 & 0 & 0 & 0 & 0 & -1 & 1 \end{bmatrix},$$

$$\Phi = \left[\Phi_i^1 \quad \Phi_j^1 \quad \Phi_i^2 \quad \Phi_j^2 \quad \Phi_i^3 \quad \Phi_j^3 \quad \Phi_i^4 \quad \Phi_j^4 \right]^T$$

In GPS baseline measurement, it is usually assumed that one end of the baseline is a known point. In epoch t , the error equation of quadratic difference obtained by synchronous observation of satellites p and q by stations i and j is

$$V_{ij}^{pq} = \frac{f}{c} \left(\frac{X_j^0 - X^q}{(\rho_j^q)_0} - \frac{X_j^0 - X^p}{(\rho_j^p)_0} \right) \delta X_j + \frac{f}{c} \left(\frac{Y_j^0 - Y^q}{(\rho_j^q)_0} - \frac{Y_j^0 - Y^p}{(\rho_j^p)_0} \right) \delta Y_j$$

$$+ \frac{f}{c} \left(\frac{Z_j^0 - Z^q}{(\rho_j^q)_0} - \frac{Z_j^0 - Z^p}{(\rho_j^p)_0} \right) \delta Z_j - N_{ij}^{pq} - I_{ij}^{pq} \tag{3}$$

where it is assumed that the coordinate of stations i is known, so $\delta X_i = \delta Y_i = \delta Z_i = 0$, The remaining terms in the error are expressed as I_{ij}^{pq} . In Eq. (3), it is assumed that the ionosphere, troposphere and other errors can be eliminated.

Furthermore, the observation equation of the quadratic difference at epoch t can be obtained

$$V = AX + L \tag{4}$$

where

$$V = [V_{ij}^{12} \ V_{ij}^{13} \ V_{ij}^{14}]^T, \quad L = [l_{ij}^{12} \ l_{ij}^{13} \ l_{ij}^{14}]^T,$$

$$X = [\delta X_{ij} \ \delta Y_{ij} \ \delta Z_{ij} \ N_{ij}^{12} \ N_{ij}^{13} \ N_{ij}^{14}]^T,$$

$$A(t) = \begin{bmatrix} \frac{1}{\lambda} \left(\frac{X_j^0 - X^2}{\rho_j^2} - \frac{X_j^0 - X^1}{\rho_j^1} \right) & \frac{1}{\lambda} \left(\frac{Y_j^0 - Y^2}{\rho_j^2} - \frac{Y_j^0 - Y^1}{\rho_j^1} \right) & \frac{1}{\lambda} \left(\frac{Z_j^0 - Z^2}{\rho_j^2} - \frac{Z_j^0 - Z^1}{\rho_j^1} \right) & 1 & 0 & 0 \\ \frac{1}{\lambda} \left(\frac{X_j^0 - X^3}{\rho_j^3} - \frac{X_j^0 - X^1}{\rho_j^1} \right) & \frac{1}{\lambda} \left(\frac{Y_j^0 - Y^3}{\rho_j^3} - \frac{Y_j^0 - Y^1}{\rho_j^1} \right) & \frac{1}{\lambda} \left(\frac{Z_j^0 - Z^3}{\rho_j^3} - \frac{Z_j^0 - Z^1}{\rho_j^1} \right) & 0 & 1 & 0 \\ \frac{1}{\lambda} \left(\frac{X_j^0 - X^4}{\rho_j^4} - \frac{X_j^0 - X^1}{\rho_j^1} \right) & \frac{1}{\lambda} \left(\frac{Y_j^0 - Y^4}{\rho_j^4} - \frac{Y_j^0 - Y^1}{\rho_j^1} \right) & \frac{1}{\lambda} \left(\frac{Z_j^0 - Z^4}{\rho_j^4} - \frac{Z_j^0 - Z^1}{\rho_j^1} \right) & 0 & 0 & 1 \end{bmatrix}$$

For m th observation epoch, the coefficient matrix of observation equation of quadratic difference can be expressed as

$$A = [A(t_1) \ A(t_2) \ \dots \ A(t_m)]^T \tag{5}$$

Using the least square method

$$V^T P V = \min \tag{6}$$

By substituting Eq. (4) into Eq. (6), and the value of δX_j , δY_j and δZ_j can be obtained. Using this method, the location of the coordinate of mobile station can be obtained.

A tensioned ground crack monitoring station was installed at the back edge where the ground cracks have been clearly developed, as shown in Fig. 9b. At the back edge, four alarms for wall cracks were set up where the rigid cracks in the Lin’s Ancestral Hall develop. Finally, since the perimeter of the landslide is not yet closed and the cracks are not arranged in an orderly manner, simple manual monitoring can be carried out at the rigid cracks of the water channel and for some local ground cracks. By attaching glass pieces to these cracks, manual check of the changes in the opening, closing, and dislocation of the glass pieces can be done regularly. This monitoring method can be adjusted dynamically according to the development of the specific situations. The layout of the monitoring locations is shown in Fig. 10.

3.2 Monitoring data and early warning guideline

The monitoring and early warning platform provides a comprehensive analysis of the monitoring data, which allows visualization of data from all monitoring locations for the landslide by specifying the time range in which the data are generated. As shown by the 3D surface displacement and rainfall monitoring data in Fig. 11, the landslide is currently in a slow creep stage, with three relatively heavy rainfall events approximately on December 15, 2020, February 10, 2021, and March 6, 2021, causing three relatively significant surface displacements, respectively.



Fig. 10 Schematic layout of landslide monitoring locations

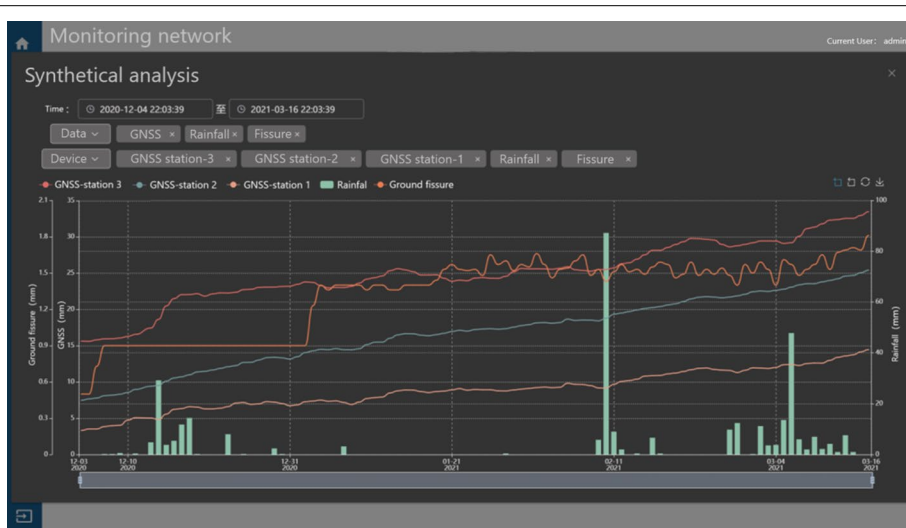


Fig. 11 GNSS 3D surface displacement and rainfall monitoring data map (December 4, 2020 to March 16, 2021)

According to the Emergency Response Law of the People's Republic of China, the early warning levels of natural disasters that can be forewarned should be divided into four levels: red, orange, yellow, and blue according to the degree of urgency, development stage, and possible harm caused by the emergency. However, there is no reference standard for the specific division of the four warning levels of geological disasters. Most experts believe that the gradient of the slope deformation–time curve can be one of the important basis for quantitative classification of slope deformation stages, and relevant scholars have proposed to predict the time of landslide initiation according to the tangent angle α which gradually converges to 90° [26]. In order to eliminate the influence of the dimension in the slope deformation–time curve, Xu et al. [27] further improved the tangent angle-based warning criterion. Most gradual landslides present initial, iso-kinetic and accelerated deformation stages, and the last stage includes low, moderate and high acceleration stages. It is proven that the tangent angle presents a significant regularity for gradual landslides [27]. In iso-kinetic deformation stage, the tangent angle remains to be 45° . In accelerated deformation stage, the tangent angle gradually increases. When it exceeds 80° , the landslide presents a rapid degradation; when it reaches 85° , the slope presents an obvious instability symptom. In this system, the improved tangent angle-based warning criterion is introduced to analyze and warn about slope stability and landslides based on real-time monitoring data, and the early warning criteria are shown in Table 1.

4 Conclusion

This study defines a monitoring and early warning system for geological disasters based on 5G communication network. While ensuring optional transmission methods such as 2G/3G/4G/GNSS, this system introduces the latest 5G communication module for the first time and uses differential chirp modulation technology to achieve low power consumption, multi-channel data return over a long distance, covering a wide range (currently up to 100 km). After receiving real-time monitoring data, this system stores, analyzes and displays multi-source heterogeneous data. Users can easily understand the monitoring indicators such as slope deformation, degree of crack development, and stress–strain situation, thus making intuitive judgments on the degree of danger due to the landslide without being distracted due to the large number of curves. In addition, the system takes into account the early warning criteria based on the tangent angle of the slope deformation–time curve and issues four levels of warnings: blue, yellow, orange, and red according to the risk level based on real-time monitoring data, which helps to realize the automation, informatization, and digitalization of geological disaster monitoring and early warning.

Table 1 Improved tangent angle criteria for landslide warning levels

Deformation stage	Uniform velocity deformation stage	Early acceleration stage	Mid-acceleration stage	Critical sliding stage
Early warning level	Attention	Caution	Warning	Danger
Warning form	Blue alert	Yellow alert	Orange alert	Red alert
Angle of incidence	$\alpha \approx 45^\circ$	$45^\circ < \alpha < 80^\circ$	$80^\circ \leq \alpha < 85^\circ$	$\alpha \geq 85^\circ$

Abbreviations

IoT: Internet of Things; GNSS: Global Navigation Satellite System; InSAR: Interferometric Synthetic Aperture Radar; GPS: Global Positioning System.

Authors' contributions

LZ was involved in the conceptualization, software, and writing—review and editing. FL was involved in the funding acquisition, project administration, and methodology. SX contributed to writing—original draft preparation. PW contributed to the validation. All authors read and approved the final manuscript.

Funding

No funding was received during this work.

Availability of data and materials

Data sharing was not applicable to this article as no datasets were generated or analyzed during the current study.

Declarations

Competing interests

All authors declare that they have no competing interests.

Author details

¹School of Civil Engineering, Yango University, Fuzhou 350015, China. ²Yunnan Innovation Institute, BUAA, Kunming 650233, China. ³School of Mechanics and Construction Engineering, China University of Mining and Technology (Beijing), Beijing 100083, China. ⁴Joint War College, National Defense University of PLA, Beijing 100091, China.

Received: 20 April 2021 Accepted: 19 July 2021

Published online: 28 July 2021

References

1. F. Lavigne, P. Wassmer, C. Gomez, T.A. Davies, D.S. Hadoko, T. Yan, The 21 February 2005, catastrophic waste avalanche at Leuwigajah dumpsite, Bandung, Indonesia. *Geoenviron. Disasters* **1**(1), 10 (2014)
2. Anuário Brasileiro de Desastres Naturais, Ministry of National Integration, National Center for Management of Risks and Disasters, Brasília, 78 (2012)
3. F.M. Guadagno, P. Revellino, G. Grelle, The 1998 Sarnolandslides: conflicting interpretations of a natural event. In: International conference on debris-flow hazards mitigation: mechanics (2001)
4. N.H. Jafari, T.D. Stark, S. Merry, The July 10, 2000 Payatas landfill slope failure. *Int. J. Geoenviron. Case Hist.* **2**(3), 208–228 (2013)
5. S. Merry, E. Kavazanjian Jr., W.U. Fritz, Reconnaissance of the July 10, 2000, Payatas landfill failure. *J. Perform. Constr. Facil.* **19**(2), 100–107 (2005)
6. Y.Y. Li, Mechanisms and kinetic behaviours of landslide and debris flow, in *Landslide Symposium* (Sichuan Science Press, 1987) **(in Chinese)**
7. C.X. Wu, L. Xu, F.C. Dai, Topographic features and initiation of earth flows on Heifangtai loess plateau. *Rock Soil Mech.* **32**(6), 1767–1773 (2011). **(in Chinese)**
8. D.X. Zhang, G.H. Wang, C.Y. Luo, J. Chen, Y.X. Zhou, A rapid loess flowslide triggered by irrigation in China. *Landslides* **6**(1), 55–60 (2009)
9. X. Yao, K. Yu, Y.S. Zhang, L.J. Li, N.J. Zhou, Mechanisms of catastrophic landslide on January 11, 2013, in Zhenxiong county: fluidization initiation and movement liquefaction of high porosity soil. *Chin. J. Rock Mech. Eng.* **33**(5), 1047–1054 (2014)
10. R.M. Yuan, C.L. Tang, J.C. Hu, X.W. Xu, Mechanism of the Donghekou landslide triggered by the 2008 Wenchuan earthquake revealed by discrete element modeling. *Nat. Hazards Earth Syst. Sci.* **14**(5), 1195–1205 (2014)
11. Y.P. Yin, C.Z. Liu, H.Q. Chen, Investigation on catastrophic landslide of January 11, 2013 at Zhaojiagou, Zhenxiong county, Yunnan province. *J. Eng. Geol.* **21**(1), 6–15 (2013)
12. Y.P. Yin, A.G. Xing, G.H. Wang, Z. Feng, B. Li, Y. Jiang, Experimental and numerical investigations of a catastrophic long-runout landslide in Zhenxiong, Yunnan, southwestern China. *Landslides* **14**(2), 649–659 (2017)
13. Q. Xu, D.L. Peng, W.L. Li, X.J. Dong, W. Hu, M.G. Tang, F.Z. Liu, The catastrophic landfill flowslide at Hongao dumpsite on 20 December 2015 in Shenzhen, China. *Nat. Hazards Earth Syst. Sci.* **17**, 277–290 (2017)
14. C.J. Ouyang, K.Q. Zhou, Q. Xu, J.H. Yin, D.L. Peng, D.P. Wang, W. Li, Dynamic analysis and numerical modeling of the 2015 catastrophic landslide of the construction waste landfill at Guangming, Shenzhen, China. *Landslides* **14**(2), 705–718 (2016)
15. Z.H. Li, Y.J. Jiang, Q. Lv, L. Sousa, M.C. He, Consistent modeling of a catastrophic flowslide at the Shenzhen landfill using a hydro-elasto-plastic model with solid-fluid transition. *Acta Geotech.* **13**(6), 1451–1466 (2018)
16. B.R. Xia, Y. Zhang, L.H. Yu, Monitoring and treatment technology of landslide geological disasters in China. *Explor. Eng. (Drill. Tunn.) (Suppl.)*, 87–90 (2001) **(in Chinese)**
17. W. Hu, S.L. Li, A study on the acoustic emission technology in the analysis of rock slope stability. *Min. Res. Dev.* **22**(3), 9–11 (2002). **(in Chinese)**
18. X.L. Wu, Y.Q. Tu, New approach of landslide activity monitoring—probing into TDR technology. *Chin. J. Rock Mech. Eng.* **21**(5), 740–744 (2002). **(in Chinese)**

19. Wan H.L.; Cai D.S.; He X.J. et al. Experimental research on monitoring deep deformation of high-steep slopes by using optical fiber sensing. *J. China Three Gorges Univ. (Nat. Sci.)* **23**(1), 20–23 (2001) **(in Chinese)**
20. X.L. Wu, Y.Q. Tu, Methods and new development of landslide activity monitoring. *China Instrum.* **1**, 10–12 (2001). **(in Chinese)**
21. C. Zhou, W.J. Chen, G.Q. Tang, Study on rock body thrust monitoring system with OTDR distributing optical fiber. *Explor. Eng. (Drill. Tunn.)* (1), 43–46 (2004) **(in Chinese)**
22. Z. Perski, H. Ramon, A. Wojcik et al., InSAR analyses of terrain deformation near the Wieliczka Salt Mine. *Poland. Eng. Geol.* (2009). <https://doi.org/10.1016/j.enggeo.2009.02.014>
23. N. Casagli, F. Cigna, S. Bianchini et al., Landslide mapping and monitoring by using radar and optical remote sensing: examples from the EC-FP7 project SAFER. *Remote Sens. Appl. Soc. Environ.* **4**, 92–108 (2016)
24. F. Bovenga, G. Pasquariello, R. Pellicani, A. Refice, G. Spilotro, Landslide monitoring for risk mitigation by using corner reflector and satellite SAR interferometry: the large landslide of Carlantino (Italy). *CATENA* **151**, 49–62 (2017)
25. M. Barla, F. Antolini, D. Bertolo, P. Thuegaz, D. D'Aria, G. Amoroso, Remote monitoring of the Comba Citrin landslide using discontinuous GBInSAR campaigns. *Eng. Geol.* **222**, 111–123 (2017)
26. J.D. Wang, Z.Y. Zhang, *The Study on Typical High-Speed Loess Landslide in Crowds Using the Systematic Analysis in Engineering Geology* (Sichuan Science Press, 1999)
27. Q. Xu, Y.P. Zeng, J.P. Qian, C.J. Wang, C.J. He, Study on a improved tangential angle and the corresponding landslide pre-warning criteria. *Geol. Bull. China* **28**(4), 501–505 (2009)
28. B. Rong, Y. Qian, K. Lu, H. Chen, M. Guizani, Call admission control optimization in WiMAX network. *IEEE Trans. Veh. Technol.* **57**(4), 2509–2522 (2008)

Publisher's Note

Springer Nature remains neutral with regard to jurisdictional claims in published maps and institutional affiliations.

Submit your manuscript to a SpringerOpen[®] journal and benefit from:

- ▶ Convenient online submission
- ▶ Rigorous peer review
- ▶ Open access: articles freely available online
- ▶ High visibility within the field
- ▶ Retaining the copyright to your article

Submit your next manuscript at ▶ [springeropen.com](https://www.springeropen.com)
